Effective protection of quantum coherence by a non-Hermitian driving potential

Kai-Qian Huang [1,2] Wen-Lei Zhao [1,*] and Zhi Li [2,†]

[1]*School of Science, Jiangxi University of Science and Technology, Ganzhou 341000, China*
[2]*Guangdong Provincial Key Laboratory of Quantum Engineering and Quantum Materials, SPTE,
South China Normal University, Guangzhou 510006, China*

We investigate the effects of non-Hermitian driving potential on quantum coherence in a bipartite system. The results show that the dynamical localization will revive after being destroyed by the Hermitian interaction, which provides evidence of the restoration of quantum coherence by a non-Hermitian driving potential. Besides, the entanglement between the two subsystems also decays with the boosting of non-Hermitian driving strength, which gives more evidence that non-Hermitian driving potential will protect quantum coherence. The physics behind this phenomenon is the domination of the quasieigenstate with maximum imaginary value of the quasieigenvalue over the dynamics of the non-Hermitian system. Our discovery establishes a restoration mechanism of quantum coherence in interacting and dissipative quantum systems which is highly expectable in updated experiments from many-body physics to quantum information.

I. INTRODUCTION

As the fingerprint of quantum coherence, localization of particles is a longstanding problem in different fields of physics, such as condensed matter physics and quantum chaos. The landmark study of Anderson discovered that the diffusion of electrons in disordered potential is frozen, which is the well-known Anderson localization (AL) [1]. The successful observation of the AL phenomenon in acoustic waves [2,3], optics [4,5], and matter waves [6,7] has proved it a universal behavior caused by wave interference. In periodically driven systems [8,9], an analog of the AL is the dynamical localization (DL) taking place in the momentum space. Interestingly, the eigenequation of the Floquet operator of δ-kick systems is mathematically equivalent to that of the Anderson model, which makes the DL established on the same footing as the AL, namely, both of them are the common phenomenon resulting from quantum coherence [10]. Remarkably, DL has already been realized in recent experiments by loading cold atoms in a periodical laser kicking [11–17], which greatly facilitates the investigation of the effects of interatomic interaction on quantum coherence and thereby leads to the appearance of novel transport phenomenon of matter waves [18].

The behaviors of quantum coherence in the presence of interatomic interaction are a fundamental problem which has potential application in the fields of quantum information and quantum computation. Previous investigations in quantum chaos have reported that the quantum coherence is fragile. As it is destroyed by sufficiently strong interaction, a wide spectrum of diffusion from the power-law diffusion $\propto t^{\alpha}$ [19–26]

to exponential diffusion $\propto e^{\beta t}$ [27–30] has been found. More recently, a theoretical study proves that any perturbation, no matter how weak it is, will be enough to destroy AL, which demonstrates the disappearance of quantum coherence and provides a solid theoretical foundation for future investigations [18]. However, the research on quantum coherence under many-body interaction is still inconclusive. Recent works report the existence of many-body localization, which indicates the appearance of quantum coherence [31]. On the other hand, the effects of interaction on quantum coherence are closely related to the fundamental problem of quantum-classical transition. It is known that the interaction with an environment even consisting of 1 degree of freedom is able to destroy quantum coherence, causing the emergence of the classically chaotic diffusion from the underlying quantum dynamics, namely, the appearance of quantum-classical correspondence (QCC) [17,32–41].

The common understanding of the quantum decoherence by interaction is based on the assumption of the Hermiticity of quantum mechanics. The rich physics in non-Hermitian systems has recently attracted extensive interest [42,43], since these intriguing behaviors in open quantum systems (e.g., optics propagation in dissipative medium, elementary excitation in condensate matter, the evolution of cold atoms with limited life span, etc.) can all be described by non-Hermitian Hamiltonians [44–48]. Exotic transport behaviors, for instance, unidirectional reflection and nonreciprocal diffraction of optics, greatly promote the exciting application of non-Hermitian physics in the actual control of light [49] and heat transport [50]. In addition, non-Hermiticity has been recognized as a fundamental modification of quantum mechanics [51,52], which opens new prospects for the theoretical physics. In this context, the novel physics of quantum coherence in the presence of interaction in non-Hermitian systems demands urgent investigation.

---

*wlzhao@jxust.edu.cn
†lizhiphys@126.com

In the present work, we study the effects of non-Hermiticity on the quantum coherence, which is displayed by the dynamics of quantum diffusion and entanglement via two coupled kicked rotors with non-Hermitian kicking potential. Interestingly, the results reveal that strong enough non-Hermitian driving can destroy the QCC of the diffusion dynamics and lead to the appearance of DL, which is the signature of the recovery of quantum coherence [53]. The entanglement of the subsystems is gradually reduced by increasing the strength of the non-Hermitian driving, even if the initial state is of maximum entanglement. The underlying physics is that an arbitrary state evolves to the quasieigenstate (QES) with the maximum imaginary part of the complex quasieigenvalue (QEV).

In the field of quantum chaos, it is widely accepted that the phenomenon of DL is the signature of quantum coherence in the diffusion dynamics [8–10]. The finding of DL has triggered extensive investigations on the issue of how the transition from quantum dynamics to classical dynamics, namely, the quantum-classical transition, occurs. Previous investigations have shown that external noises [54] and coupling [17,32–40] with environment can lead to the delocalization and the QCC of diffusion, which is caused by the quantum decoherence effects from the noises or the coupling. Taking this into account, our result clearly demonstrates the protection of quantum coherence by the non-Hermitian kicking potential, which is a meaningful discovery in the fields of quantum information and quantum chaos. More recently, the phenomenon of DL has been realized in a quantum hardware, where the quantum coherence is crucial to ensure the validity of the quantum simulations [55]. It is known that quantum coherence is an important resource in quantum technology. For example, in quantum error-correcting codes, the main issue is to protect the quantum coherence of the subsystem and prevent the leaking of information to the environment. In quantum teleportation, one should also protect the information of the system and reduce the decoherence effects of the environment [55–59]. Therefore, our finding of the mechanism of protection by Floquet driving may be of fundamental interest in the fantastic fields of quantum computation and quantum communication.

The paper is organized as follows. In Sec. II, we describe our model and show the phenomenon of dynamical localization induced by a non-Hermitian driving potential. In Sec. III, we show our theoretical analysis. A summary is presented in Sec. IV.

II. MODEL AND RESULTS

The Hamiltonian of the bipartite system reads

$$H = H_1 + H_2 + H_I, \qquad (1)$$

where H_j ($j = 1$ and 2) represents the Hamiltonian of individual particles, and H_I is the interaction. Each subsystem is a kicked rotor for which the Hamiltonian takes the form

$$H_j = \frac{p_j{}^2}{2} + V_K(\theta_j) \sum_n \delta(t - t_n), \qquad (2)$$

with

$$V_K(\theta_j) = (K_j + i\lambda_j)\cos(\theta_j), \qquad (3)$$

where p_j is the angular momentum operator, θ_j is the angle coordinate, K_j denotes the strength of the real part of the kicking potential, and λ_j is the strength of its imaginary part. The interacting part reads

$$H_I = \varepsilon \hbar_{\mathrm{eff}} \cos(\theta_1)\cos(\theta_2) \sum_n \delta(t - t_n), \qquad (4)$$

with ε being the interaction strength and $\hbar_{\mathrm{eff}}$ being the effective Plank constant. All quantities are in dimensionless units. An arbitrary state can be expanded on the basis of the product states of the eigenstates of unperturbed rotors, i.e., $|\psi\rangle = \sum_{m,n} \psi_{m,n}|m, n\rangle$ with $p|n\rangle = n\hbar_{\mathrm{eff}}|n\rangle$ and $\langle\theta|n\rangle = e^{in\theta}/\sqrt{2\pi}$. The time evolution from $t = t_n$ to $t = t_{n+1}$ is governed by the Floquet operator $|\psi(t_{n+1})\rangle = U|\psi(t_n)\rangle$. Due to the δ kick, the Floquet operator can be separated into two fractions,

$$U = U_f U_K, \qquad (5)$$

where the evolution operator of the kinetic term takes the form

$$U_f = \exp\left(-\frac{i}{\hbar_{\mathrm{eff}}} \sum_{j=1}^{2} \frac{p_j^2}{2}\right), \qquad (6)$$

and for the kick term it is

$$U_K = \exp\left[-\frac{i}{\hbar_{\mathrm{eff}}} \sum_{j=1}^{2} V_K(\theta_j) - \frac{i}{\hbar_{\mathrm{eff}}} H_I(\theta_1, \theta_2)\right]. \qquad (7)$$

The non-Hermitian extension of the kicked rotor model has been previously introduced to demonstrate the $\mathcal{PT}$-symmetric phase breaking in the Floquet system [60] and the non-Hermitian effects on Floquet topological phases [61]. Based on this, we make a generalization of the coupled kicked rotors to the non-Hermitian regime, with which we can investigate the entanglement in non-Hermitian chaotic systems [62,63]. Although the decoherence-induced QCC in a system of coupled-Hermitian kicked rotors has been tentatively experimented with [17], the experimental realization of the case with the non-Hermitian kicking potential in Eq. (3) still remains untouched; therefore, our present work is particularly valuable as theoretical progress. Actually, experimental advances in both optics [44–48] and cold atoms [64–66] have unveiled exotic phenomena in non-Hermitian systems, for instance, the topological states [47] and the Floquet solitons [48]. The periodical modulation of dissipation and coupling in ultracold atoms has been used to experimentally engineer the $\mathcal{PT}$-symmetric phase transition [45]; therefore, we hope that our theoretical model will be verified by further experiments.

To quantify the quantum diffusion, we have

$$\langle p_1^2 \rangle = \mathrm{Tr}(\rho_1 p_1^2), \qquad (8)$$

which is marked as particle 1, with

$$\rho_1 = \frac{1}{\mathcal{N}}\mathrm{Tr}_2(|\psi\rangle\langle\psi|), \qquad (9)$$

where ρ_1 is the reduced density matrix by partial matrix tracing on the density matrix of the two-particle system $\rho = |\psi\rangle\langle\psi|$, and $\mathcal{N}$ is the norm of quantum states. Note that the
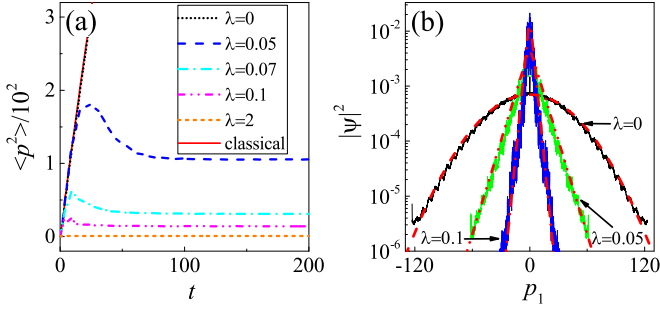
FIG. 1. (a) Time dependence of the mean energy for particle 1 $\langle p_1^2 \rangle$. The corresponding λ values are given. (b) Probability density distribution in the momentum space for particle 1 $|\psi_1|^2$ at the time $t_n = 100$. The fitting curves are the Gaussian function of the form $|\psi(p_1)|^2 \propto \exp(-p_1^2/\sigma)$ with $\sigma \approx 2500$ (dashed line) and the exponential localization $|\psi(p_1)|^2 \propto \exp(-|p_1|/\zeta)$ with $\zeta \approx 2.5$ (dash-dotted line) and 7.7 (dash-dot-dotted line). The parameters are $K = 5.0$, $\varepsilon = 5$, and $\hbar_{\text{eff}} = 0.06$.

value of $\mathcal{N}$ will exponentially increase due to the appearance of complex QEVs for sufficiently strong non-Hermitian kicking. Therefore, the above definition of the expectation value $\langle p_1^2 \rangle$ reduces the contribution of the growth from the norm. In numerical simulation, we set the initial state as the product state of the ground state $|\psi(t_0)\rangle = |00\rangle$. Without loss of generality, we consider the case with $K_1 = K_2 = K$ and $\lambda_1 = \lambda_2 = \lambda$; namely, the two particles are identical. We also investigate the case with $\lambda_1 = 0$ and $\lambda_2 \neq 0$, which simulates the case of a Hermitian particle experiencing the non-Hermitian effect, and we find that there are no essential differences with $\lambda_1 = \lambda_2$.

Previous investigations on the Hermitian systems (i.e., $\lambda = 0$) have reported that the two-particle interaction is able to destroy the quantum coherence if the interaction is strong enough [17,32–40]. As a consequence, the quantum diffusion is in consistence with its classical counterpart, i.e., the QCC. In the Hermitian case, the classical dynamics is governed by the mapping equation, which allows us to numerically investigate the classical dynamics [67]. We consider the case that the kick strength of the two particles is strong enough, i.e., $K = 5$, so that the classical dynamics is fully chaotic. The QCC of the Hermitian case is shown in Fig. 1(a), where one can see that both the classical and the quantum mean energy of particle 1 increase linearly with time, i.e., $\langle p_1^2(t) \rangle = Dt$. In addition, the diffusion coefficient D almost equals that of a single kicked rotor, i.e., $D \approx K^2/2$, because in our model the interaction strength is negligibly small in the semiclassical limits, i.e., $\hbar_{\text{eff}} \ll 1$ [see Eq. (4)]. It is worth noting that the linear increase of the mean square of momentum, which is traditionally termed as normal diffusion, is a character of chaotic behavior. We further investigate the momentum distribution for the appearance of QCC. Our results show that the momentum distribution is in the form of the Gaussian function $|\psi(p_1)|^2 \propto \exp(-p_1^2/\sigma)$, which is the brand mark of chaotic diffusion in the momentum space and demonstrates the disappearance of quantum coherence due to the interaction [see Fig. 1(b) for $\lambda = 0$].

Interestingly, for a specific value of λ [e.g., $\lambda = 0.05$ in Fig. 1(a)], the quantum diffusion of the system complies with
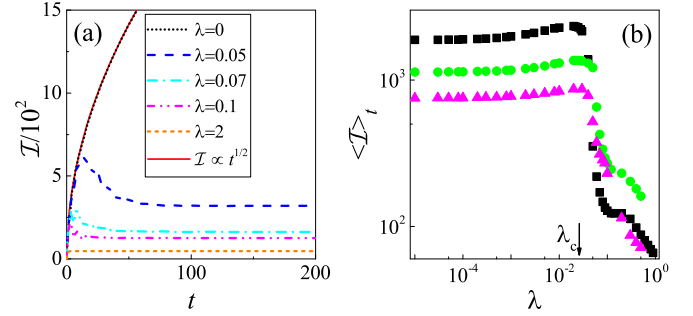
FIG. 2. (a) Time dependence of the IPR with $\hbar_{\text{eff}} = 0.06$. The corresponding λ values are given. (b) Time-averaged IPR $\langle \mathcal{I} \rangle_t$ versus λ with $\hbar_{\text{eff}} = 0.06$ (squares), 0.1 (circles), and 0.15 (triangles). The arrow marks the threshold value of λ_c. Other parameters are the same as those in Fig. 1.

the classically chaotic diffusion during a finite time interval, after which it will gradually approach saturation. This clearly demonstrates the appearance of DL. From Fig. 1(a), one can also see that the saturation value of $\langle p_1^2 \rangle$ decreases with the increase of λ, which demonstrates that the extent of DL grows as the strength of the non-Hermitian driving potential increases [53]. To confirm the appearance of DL, we numerically investigate the momentum distribution at the time when the mean value $\langle p_1^2 \rangle$ saturates. Our results show that the quantum state is exponentially localized in the momentum space, i.e., $|\psi(p_1)|^2 \propto \exp(-|p_1|/\zeta)$ [see Fig. 1(b) for $\lambda = 0.05$], which is in sharp contrast with the Gaussian distribution in the presence of QCC. Moreover, the localization length ζ decreases with the increase of λ [see Fig. 1(b) for $\lambda = 0.1$], which is consistent with the tendency of the mean energy $\langle p_1^2 \rangle$ with the increase of λ, and thus is clear evidence of DL.

In order to quantify the localization of the wave packet, we numerically investigate the inverse participation ratio (IPR),

$$\mathcal{I} = \frac{\left(\sum_n |\psi_n|^2 \right)^2}{\sum_n |\psi_n|^4}. \tag{10}$$

In the Hermitian case, the subsystem displays classically chaotic diffusion for which the time-dependent probability distribution is in the Gaussian form, i.e., $|\psi(p)|^2 = \exp[-p^2/(K^2 t)]/(K^2 \pi t)^{1/2}$, with p being the momentum and K being the kicking strength. It is then straightforward to get an approximated expression of the IPR, i.e., $\mathcal{I} \approx (\int_{-\infty}^{+\infty} |\psi(p)|^4 dp)^{-1} \propto \sqrt{t}$ [see $\lambda = 0$ in Fig. 2(a)], where we have used the normalization condition $\sum_n |\psi_n|^2 = 1$. For a specific λ value (e.g., $\lambda = 0.05$), the IPR shows again a power-law increase for a finite time interval, after which it gradually saturates. Remember that for the same strength of non-Hermitian kicking potential, the quantum state is exponentially localized in the momentum space, i.e., $|\psi(p_1)|^2 \propto \exp(-|p_1|/\zeta)$ [see Fig. 1(b)]. The saturation value of IPR is virtually proportional to the localization length of the quantum state, i.e., $\mathcal{I} \approx 1/\sum_{p_1} |\psi(p_1)|^4 \simeq \zeta$. We further numerically investigate the time-averaged value of the IPR, $\langle \mathcal{I} \rangle_t = \frac{1}{t_f} \int_0^{t_f} \mathcal{I}(t) dt$ for different λ values. It is worth noting that, in the Hermitian case, the value of $\langle \mathcal{I} \rangle_t$ is dependent on t_f since $\langle \mathcal{I} \rangle_t \propto \frac{1}{t_f} \int_0^{t_f} \sqrt{t} dt \propto \sqrt{t_f}$. In numerical simulations, we
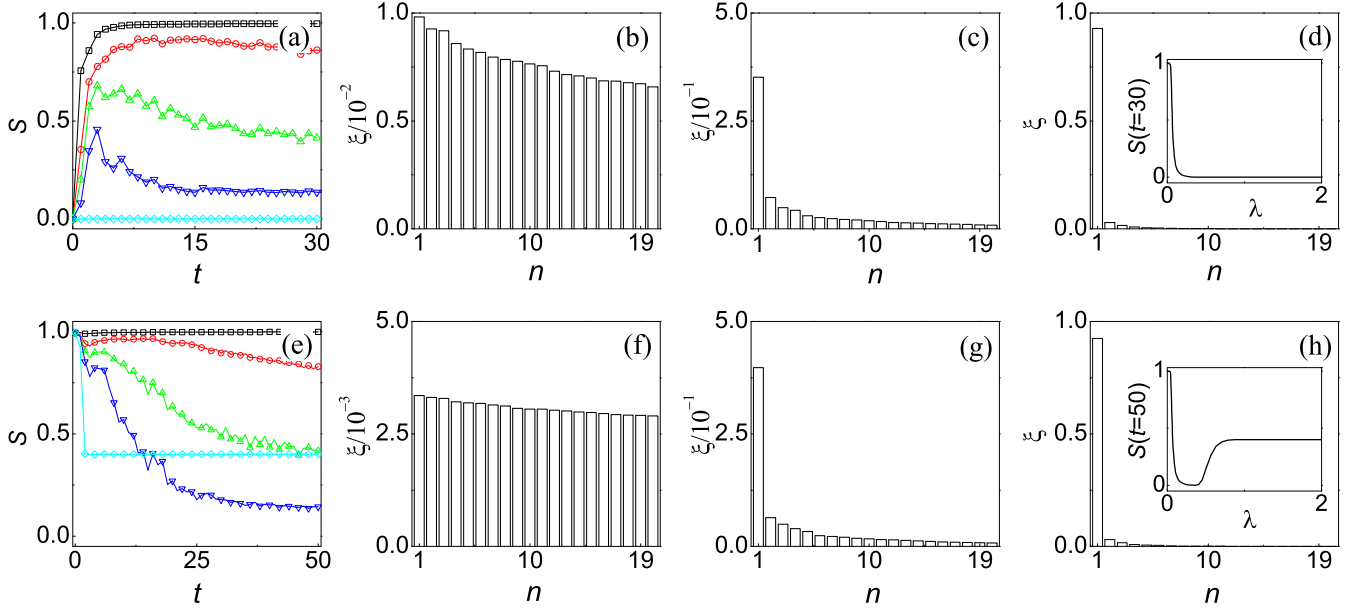
FIG. 3. (a) Linear entropy S versus time with $\lambda = 0.0$ (squares), 0.05 (circles), 0.07 (up triangles), 0.1 (down triangles), and 1 (diamonds). (b)–(d) The eigenvalue ξ of the reduced density operator ρ_1 at the time $t_n = 30$ with $\lambda = 0$ (b), 0.05 (c), and 0.1 (d). Inset in panel (d): Dependence of S at the time $t_n = 30$ on λ. The initial state is a product state of the ground state $|\psi(t_0)\rangle = |00\rangle$. Bottom panels are the same as in the above but for an initial state with the maximum entanglement, i.e., $|\psi(t_0)\rangle = \sum \psi_{n,n+1}|n, n+1\rangle$, with $\psi_{n,n+1} = \mathcal{N}_0 e^{-n^2/\sigma}$ and $\sigma = 12\,000$. In panel (e), $\lambda = 0.0$ (squares), 0.05 (circles), 0.07 (up triangles), 0.1 (down triangles), and 1 (diamonds). In panels (f)–(h), the eigenvalue ξ of ρ_1 at the time $t_n = 50$ for $\lambda = 0.0$ (f), 0.05 (g), and 0.1 (h). Inset in panel (h): S at the time $t_n = 50$ versus λ. Other parameters are the same as those in Fig. 1.

use two hundred kicks, i.e., $t_f = 200$ to calculate $\langle \mathcal{I} \rangle_t$, which is long enough to get the highly precise value of the saturation of $\mathcal{I}$ with large λ, as $\mathcal{I}$ rapidly saturates with time. Figure 2(b) shows that, for a specific $\hbar_{\mathrm{eff}}$, $\langle \mathcal{I} \rangle_t$ has a plateau for small λ, and after a threshold λ_c it decreases with λ. The region of plateau corresponds to the $\langle \mathcal{I} \rangle_t$ of the Hermitian case, because for $\lambda < \lambda_c$ the quasienergies are all real. For $\lambda > \lambda_c$, some of the quasienergies become complex. Moreover, the number of these complex quasienergies increases with the increase of λ. In this regime, a quantum state rapidly evolves to the quasieigenstate with maximum imaginary quasienergy, which is exponentially localized in the momentum space [see Fig. 4(b)]. Our result clearly demonstrates that there is a threshold λ_c value corresponding to the appearance of DL.

It is known that during the process of QCC the entanglement between the subsystems grows. A commonly used quantity to measure the entanglement is the linear entropy

$$S(t) = 1 - \mathrm{Tr}\left[\rho_1^2(t)\right]. \tag{11}$$

With the generation of entanglement, a pure state evolves to a mixed one, correspondingly the value of S increases from zero to almost unity [68,69] [see Fig. 3(a) for $\lambda = 0$]. This process is accompanied by the disappearance of quantum coherence. Therefore, it is believed that the decoherence effects induced by interaction result in the QCC of diffusion dynamics. Our results show that, for a specific λ value, the linear entropy rapidly increases to saturation over time [see Fig. 3(a) for $\lambda = 0.05$]. Interestingly, the saturation value decreases with the increase of λ, and is almost zero for sufficiently large λ [see the inset in Fig. 3(d)], which clearly demonstrates that the non-Hermitian driving potential can reduce the entanglement

of the system. As a further step, we numerically investigate the eigenvalue ξ of the reduced density operator ρ_1 at the time when the linear entropy saturates. Our results show that for small λ [e.g., $\lambda = 0.05$ in Fig. 3(b)], there are many eigenvalues. For an intermediate value of λ [e.g., $\lambda = 0.07$ in Fig. 3(c)], the number of ξ with large values reduces. For large λ [e.g., $\lambda = 0.1$ in Fig. 3(d)], there is a ξ whose value is almost unity, i.e., $\xi \approx 1$. Note that the wide distribution of
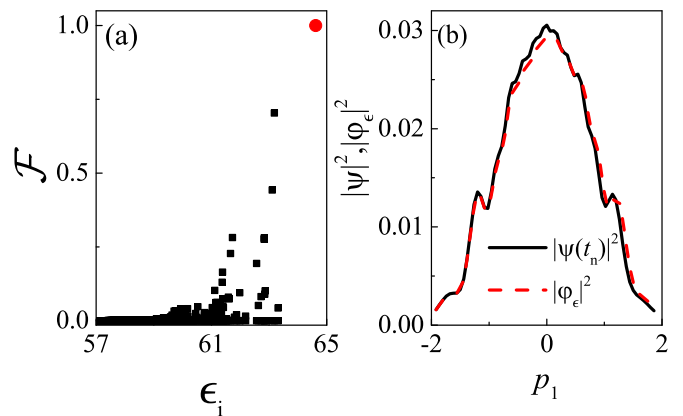

FIG. 4. (a) Fidelity $\mathcal{F} = |\langle \varphi_\epsilon | \psi(t_n) \rangle|^2$ between the QESs $|\varphi_\epsilon\rangle$ and the quantum state $|\psi(t_n)\rangle$ with $t_n = 100$. The red (gray) dot marks the value of $\mathcal{F} \approx 1$ corresponding to the maximum value of $\epsilon_i = 64.62$. (b) Comparison of momentum distributions between the QES $|\varphi_\epsilon\rangle$ with $\epsilon_i = 64.62$ (dashed line) and the quantum state $|\psi(t_n = 100)\rangle$ (solid line). The value of λ is $\lambda = 2.0$. Other parameters are the same as those in Fig. 1.

ξ indicates that the time-evolved quantum state is a mixed state [70,71]. For the appearance of an eigenvalue of unity, the quantum state becomes actually a pure state. Therefore, our results demonstrate the transition of a quantum state from the mixed state to an almost pure state as the strength of the non-Hermitian kicking potential increases. It is a strong evidence that the non-Hermitian driving potential effectively protects the quantum coherence.

We further consider the case that the initial state is of maximum entanglement, i.e., $|\psi(t_0)\rangle = \sum \psi_{n,n+1}|n, n+1\rangle$, for which the component is in the distribution of the Gaussian function $\psi_{n,n+1} = \mathcal{N}_0 e^{-n^2/\sigma}$, with $\mathcal{N}_0$ being the normalization constant and $\sigma = 12\,000$. The value of the linear entropy of this state is unity, i.e., $S(t_0) = 1$. We find that for $\lambda = 0$ the value of S remains unity, i.e., $S = 1$, as time evolves. For small λ [e.g., $\lambda = 0.05$ in Fig. 3(e)], the value of S decays from unity with time evolution. For larger values of λ [e.g., $\lambda = 0.07$ and 0.1 in Fig. 3(e)], the value of S rapidly decays from unity to saturation. We further investigate the saturation value of S for different λ values. Our numerical results show that, for λ values smaller than a threshold value $\lambda < \lambda_c$, the saturation value decreases from unity to almost zero with the increase of λ, and for $\lambda > \lambda_c$ it increases to a fixed value with an increasing λ [see the inset in Fig. 3(h)]. It clearly demonstrates that the quantum coherence recovers with the increase of the non-Hermitian driving potential. To confirm this finding, we numerically investigate the eigenvalue of ρ_1 when the linear entropy saturates. Our numerical results show that, with the increase of λ, the number of relatively large ξ decreases, and for sufficiently large λ there is a ξ value equal to almost unity [see Figs. 3(f)–3(h)]. This again demonstrates the transition from a mixed state to a pure state under the effects of the non-Hermitian driving potential, which is the signature of the recovery of quantum coherence.

III. THEORETICAL ANALYSIS

The eigenequation of the Floquet operator has the expression $U|\varphi_\epsilon\rangle = e^{-i\epsilon}|\varphi_\epsilon\rangle$, where ϵ is the QEV and $|\varphi_\epsilon\rangle$ is the corresponding QES. At the initial time, an arbitrary state can be expanded on the basis of the QESs, namely, $|\psi(t_0)\rangle = \sum_\epsilon C_\epsilon|\varphi_\epsilon\rangle$. After the nth kick, the expansion of the state takes the form $|\psi(t_n)\rangle = U^n|\psi(t_0)\rangle = \sum_\epsilon C_\epsilon e^{-in\epsilon}|\varphi_\epsilon\rangle$. It is worth noting that the QEVs become complex, i.e., $\epsilon = \epsilon_r + i\epsilon_i$ in the condition that the λ value is large enough. Accordingly, one can get $|\psi(t_n)\rangle = \sum_\epsilon C_\epsilon e^{n\epsilon_i} e^{-in\epsilon_r}|\varphi_\epsilon\rangle$. With time evolution, the components $C_\epsilon e^{n\epsilon_i}$ with $\epsilon_i > 0$ will exponentially increase, and that of negative ϵ_i exponentially decays. So, the quantum state $|\psi(t_n)\rangle$ will eventually evolve to the QES with the maximum ϵ_i. To confirm our analysis, we numerically investigate the fidelity between the QESs and the time-evolved state $\mathcal{F} = |\langle\varphi_\epsilon|\psi(t_n)\rangle|^2$ when DL appears while the linear entropy is almost zero for large enough λ values [e.g., $t_n = 100$ and $\lambda = 2.0$ in Fig. 4(a)]. Our result shows that the value of $\mathcal{F}$ is almost unity corresponding to the maximum value of ϵ_i, i.e., $\epsilon_i^{max} = 64.62$ [see Fig. 4(a)], which demonstrates the coincidence of the quantum state with the QESs of ϵ_i^{max}. Note that the QESs with complex QEVs are not orthogonal,; hence, there are some nonzero values of $\mathcal{F}$. We further display both the quantum state $|\psi(t_n)\rangle$ and the QES $|\varphi_{\epsilon_i}\rangle$ of ϵ_i^{max}

in the momentum space. The results again suggest that the two states are in perfect agreement with each other, both of which are extremely localized in the momentum space [see Fig. 4(b)]. Therefore, the appearance of DL is rooted in the localization of the QES with maximum ϵ_i. As the localization length of this QES is very small, it can be safely regarded as a pure state, which preserves the quantum coherence; hence, the linear entropy is nearly zero [see the inset in Fig. 3(e)]. Even if we select a state with the maximum entanglement, it will rapidly evolve to the QES of maximum ϵ_i. This process corresponds to the decay of linear entropy from unity to a saturation level as shown in Fig. 3(e). So the recovery of quantum coherence in the coupled bipartite system is due to the fact that the quantum states evolve to a QES with a maximum value of the imaginary QEV. Moreover, this QES is virtually a pure state. Our finding establishes a different mechanism of decoupling by the non-Hermitian kick potential, which results in the restoration of quantum coherence and is in some sense universal in non-Hermitian periodical driven systems [67].

IV. SUMMARY

In this work, we investigate the dynamics of the quantum diffusion and entanglement in a bipartite system with a non-Hermitian kicking potential. For a strong enough λ value, the quantum diffusion of $\langle p_1^2 \rangle$ follows the classically chaotic way during the short time interval, after which it saturates. The saturation values of $\langle p_1^2 \rangle$ decrease with the increase of λ, which clearly demonstrates the enhancement of DL by the non-Hermitian driving potential. The formation of DL corresponds to the reducing of entanglement between the two subsystems, for which the saturation level of linear entropy decreases with the increase of λ. On the other hand, for maximum entanglement states, the linear entropy will decay from 1 to almost 0 during the evolving process, which again suggests the recovery of quantum coherence. As a consequence, the time-evolved state becomes a pure state, which is characterized by the formation of one significantly large eigenvalue of the reduced density matrix. The mechanism is that a quantum state finally evolves to a QES whose imaginary part of the QEV is maximum. Our investigation reveals that non-Hermiticity is useful to protect quantum coherence, which provides new insights in the fields of quantum information and quantum chaos.

APPENDIX A: CLASSICAL AND QUANTUM PHASE SPACE

In the Hermitian case, the classical mapping equations of the two-coupled kicked rotors read

$$p_1^{n+1} - p_1^n = K \sin(\theta_1^n) + \varepsilon \sin(\theta_1^n)\cos(\theta_2^n), \qquad \text{(A1)}$$
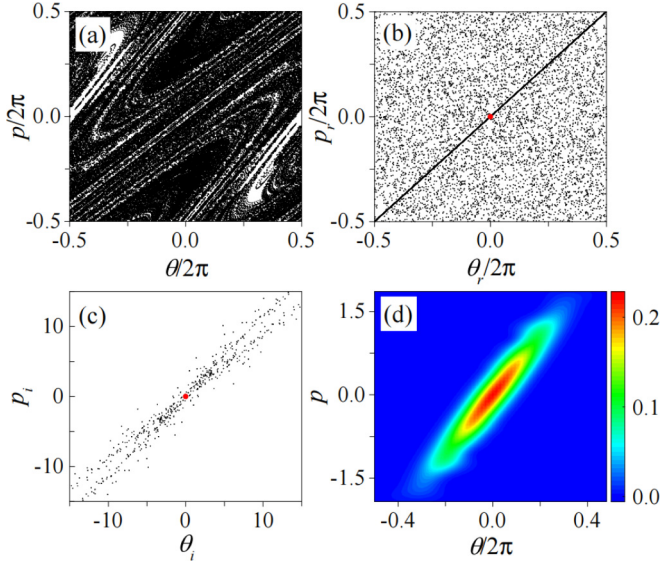
FIG. 5. (a)–(c) Phase-space portrait of particle 1 of our model at the time $t_n = 4$ with $K = 5$ and $\varepsilon = 0.3$. Panel (a) shows (p, θ) with $\lambda = 0$. Panels (b) and (c) show (p_r, θ_r) and (p_i, θ_i) with $\lambda = 2$. The red (gray) dots represent the fixed points with $p_r = \theta_r = 0$ and $p_i = \theta_i = 0$. (d) Husimi distribution $|\langle \Psi | \varphi_\epsilon \rangle|^2$ of the QES with $\epsilon_i = 64.62$ and $\lambda = 2$ [see the dashed line in Fig. 4(b)]. Other parameters are the same as those in Fig. 1.

$$\theta_1^{n+1} - \theta_1^n = p_1^{n+1}, \tag{A2}$$

$$p_2^{n+1} - p_2^n = K \sin\left(\theta_2^n\right) + \varepsilon \cos\left(\theta_1^n\right) \sin\left(\theta_2^n\right), \tag{A3}$$

$$\theta_2^{n+1} - \theta_2^n = p_2^{n+1}. \tag{A4}$$

where p_i^n (θ_i^n) represents the angular momentum (coordinate) of the ith particle at the time $t = t_n$. We numerically investigate the phase space for an ensemble of 200 000 trajectories with the initial values θ_1^0 and θ_2^0 being uniformly distributed in $[-\pi, \pi]$, and $p_1^0 = p_2^0 = 0$. Because the two rotors are identical, we plot the phase-space portrait of particle 1 (θ_1^n, p_1^n) in Fig. 5(a). One can find that the classical phase space is almost occupied by chaotic diffusion of trajectories, demonstrating the chaotic dynamics of the system.

In the non-Hermitian case, one can extend the Hamilton canonical equation to get the following mapping equations [72–77]:

$$p_1^{n+1} - p_1^n = (K + i\lambda) \sin\left(\theta_1^n\right) + \varepsilon \sin\left(\theta_1^n\right) \cos\left(\theta_2^n\right), \tag{A5}$$

$$\theta_1^{n+1} - \theta_1^n = p_1^{n+1}, \tag{A6}$$

$$p_2^{n+1} - p_2^n = (K + i\lambda) \sin\left(\theta_2^n\right) + \varepsilon \cos\left(\theta_1^n\right) \sin\left(\theta_2^n\right), \tag{A7}$$

$$\theta_2^{n+1} - \theta_2^n = p_2^{n+1}. \tag{A8}$$

In addition, the classical trajectories are complex [72–77],

$$p_j^n = p_{j,r}^n + i p_{j,i}^n, \tag{A9}$$

$$\theta_j^n = \theta_{j,r}^n + i \theta_{j,i}^n, \tag{A10}$$

where $p_{j,r}^n$ $(p_{j,i}^n)$ denotes the real (imaginary) part of the angular momentum of the jth particle, and $\theta_{j,r}^n$ $(\theta_{j,i}^n)$ is the corresponding angular coordinate. Plugging Eqs. (A9) and (A10) into Eqs. (A5)–(A8) yields the following mapping equations:

$$\begin{aligned} p_{1,r}^{n+1} - p_{1,r}^n = {} & K \sin\left(\theta_{1,r}^n\right) \cosh\left(\theta_{1,i}^n\right) - \lambda \cos\left(\theta_{1,r}^n\right) \sinh\left(\theta_{1,i}^n\right) \\ & + \varepsilon[\sin\left(\theta_{1,r}^n\right) \cosh\left(\theta_{1,i}^n\right) \cos\left(\theta_{2,r}^n\right) \cosh\left(\theta_{2,i}^n\right) + \cos\left(\theta_{1,r}^n\right) \sinh\left(\theta_{1,i}^n\right) \sin\left(\theta_{2,r}^n\right) \sinh\left(\theta_{2,i}^n\right)], \end{aligned} \tag{A11}$$

$$\begin{aligned} p_{1,i}^{n+1} - p_{1,i}^n = {} & K \cos\left(\theta_{1,r}^n\right) \sinh\left(\theta_{1,i}^n\right) + \lambda \sin\left(\theta_{1,r}^n\right) \cosh\left(\theta_{1,i}^n\right) \\ & + \varepsilon[\cos\left(\theta_{1,r}^n\right) \sinh\left(\theta_{1,i}^n\right) \cos\left(\theta_{2,r}^n\right) \cosh\left(\theta_{2,i}^n\right) - \sin\left(\theta_{2,r}^n\right) \sinh\left(\theta_{2,i}^n\right) \sin\left(\theta_{1,r}^n\right) \cosh\left(\theta_{1,i}^n\right)], \end{aligned} \tag{A12}$$

$$\theta_{1,r}^{n+1} - \theta_{1,r}^n = p_{1,r}^{n+1}, \tag{A13}$$

$$\theta_{1,i}^{n+1} - \theta_{1,i}^n = p_{1,i}^{n+1}, \tag{A14}$$

$$\begin{aligned} p_{2,r}^{n+1} - p_{2,r}^n = {} & K \sin\left(\theta_{2,r}^n\right) \cosh\left(\theta_{2,i}^n\right) - \lambda \cos\left(\theta_{2,r}^n\right) \sinh\left(\theta_{2,i}^n\right) \\ & + \varepsilon\left[\sin\left(\theta_{2,r}^n\right) \cosh\left(\theta_{2,i}^n\right) \cos\left(\theta_{1,r}^n\right) \cosh\left(\theta_{1,i}^n\right) + \cos\left(\theta_{2,r}^n\right) \sinh\left(\theta_{2,i}^n\right) \sin\left(\theta_{1,r}^n\right) \sinh\left(\theta_{1,i}^n\right) \right], \end{aligned} \tag{A15}$$

$$\begin{aligned} p_{2,i}^{n+1} - p_{2,i}^n = {} & K \cos\left(\theta_{2,r}^n\right) \sinh\left(\theta_{2,i}^n\right) + \lambda \sin\left(\theta_{2,r}^n\right) \cosh\left(\theta_{2,i}^n\right) \\ & + \varepsilon\left[\cos\left(\theta_{2,r}^n\right) \sinh\left(\theta_{2,i}^n\right) \cos\left(\theta_{1,r}^n\right) \cosh\left(\theta_{1,i}^n\right) - \sin\left(\theta_{1,r}^n\right) \sinh\left(\theta_{1,i}^n\right) \sin\left(\theta_{2,r}^n\right) \cosh\left(\theta_{2,i}^n\right) \right], \end{aligned} \tag{A16}$$

$$\theta_{2,r}^{n+1} - \theta_{2,r}^n = p_{2,r}^{n+1}, \tag{A17}$$

$$\theta_{2,i}^{n+1} - \theta_{2,i}^n = p_{2,i}^{n+1}. \tag{A18}$$

Straightforward analysis of the above equation can reveal a fixed point, i.e., $\theta_{1,r}^n = \theta_{1,i}^n = \theta_{2,r}^n = \theta_{2,i}^n = 0$ and $p_{1,r}^n = $ $p_{1,i}^n = p_{2,r}^n = p_{2,i}^n = 0$ [see Figs. 5(b) and 5(c)]. We make an extension of the traditional definition of the phase space to
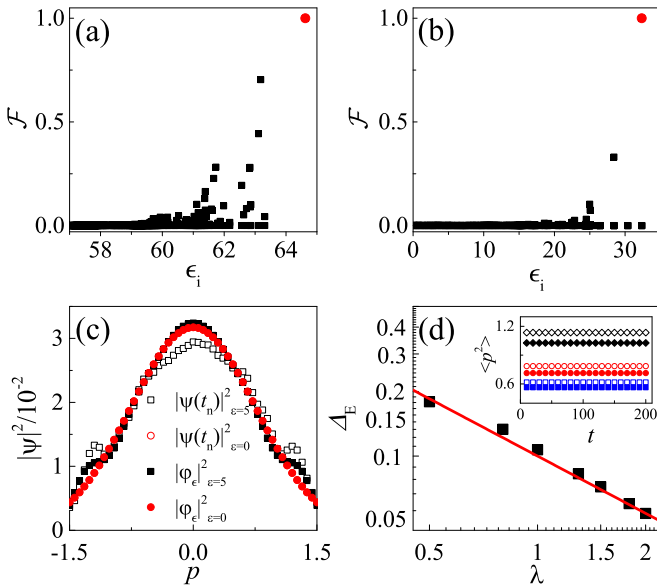
FIG. 6. Top panels: Fidelity $\mathcal{F} = |\langle \varphi_\epsilon | \psi(t_n) \rangle|^2$ between the QESs $|\varphi_\epsilon\rangle$ and the quantum state $|\psi(t_n = 100)\rangle$ with $\varepsilon = 5$ (a) and 0 (b) for $\lambda = 2$. The red (gray) dots mark the maximum value of $\mathcal{F}$, i.e., $\mathcal{F} \approx 1$, which corresponds to the maximum ϵ_i, i.e., $\epsilon_i = 64.62$ in panel (a) and $\epsilon_i = 32.35$ in panel (b). (c) Comparison of probability density distributions in momentum space for the four states with maximum $\mathcal{F}$: two QESs $|\varphi_\epsilon\rangle$ with ($\varepsilon = 5$, $\epsilon_i = 64.62$) (solid squares) and ($\varepsilon = 0$, $\epsilon_i = 32.35$) (solid circles); two quantum states $|\psi(t_n = 100)\rangle$ with $\varepsilon = 5$ (empty squares) and $\varepsilon = 0$ (empty circles). (d) The difference Δ_E of $\langle p^2(t) \rangle$ between $\varepsilon = 0$ and 5 versus λ. The red (gray) line denotes the power-law decay, i.e., $\Delta_E \approx \lambda^{-\beta}$ with $\beta \approx 0.89$. Inset: Time dependence of $\langle p^2 \rangle$ with $\varepsilon = 0$ (solid symbols) and $\varepsilon = 5$ (empty symbols). From top to bottom, the symbols correspond to $\lambda = 1$ (diamonds), 1.5 (circles), and 2 (squares). Other parameters are the same as those in Fig. 1.

be (p_r, θ_r) and (p_i, θ_i) with respect to the complex trajectories. In numerical simulations, we set the initial trajectory as $\theta_{1,i}^0 = \theta_{2,i}^0 = p_{1,r}^0 = p_{2,r}^0 = p_{1,i}^0 = p_{2,i}^0 = 0$, and $\theta_{1,r}^0$ and $\theta_{2,r}^0$ are distributed uniformly in the interval $[-\pi, \pi]$. Figure 5(b) shows that the phase space (p_r, θ_r) is chaotic, except for a fixed point $(p_r = 0, \theta_r = 0)$ and a regular trajectory $(p_r = \theta_r)$. Interestingly, the phase space of the imaginary trajectories (p_i, θ_i) exhibits the diffusion around the trajectory $p_i = \theta_i$, which has been reported in our previous investigations in Ref. [53].

To investigate the fingerprint of the classical phase space on quantum dynamics, we numerically investigate the Husimi distribution $|\langle \Psi(\theta_0, p_0) | \varphi_\epsilon \rangle|^2$ of the QES, where $|\Psi(\theta_0, p_0)\rangle = (\frac{\alpha}{\pi})^{\frac{1}{4}} \exp[-\frac{\alpha}{2}(\theta - \theta_0)^2 + i\frac{p_0}{\hbar_{eff}}\theta]$ is the coherent state centered at (θ_0, p_0) with $\alpha = 10$, and $|\varphi_\epsilon\rangle$ is the QES. We focus on the case with $\lambda \geqslant \lambda_c$ so that the QESs are well

localized in the momentum space [i.e., $\lambda = 2$ in Fig. 4(b)]). Interestingly, the Husimi distribution is centered at ($p_0 = 0$, $\theta_0 = 0$), which is just the fixed point of the classical phase space. Moreover, the configuration of the Husimi distribution is similar to that of the phase space (p_i, θ_i) of imaginary trajectories [see Figs. 5(c) and 5(d)]. This kind of connection may have important insights into the quantum-classical correspondence of chaotic systems.

APPENDIX B: DECOUPLING EFFECTS BY NON-HERMITIAN KICKING POTENTIAL

Our results in Fig. 3 show that the non-Hermitian kicking potential effectively suppresses the entanglement of subsystems. This reveals that the non-Hermitian kicking potential induces decoupling effects in the system. To confirm this issue, we compare the dynamics of a subsystem between $\varepsilon = 0$ and 5 for large enough λ values. We numerically investigate the fidelity between the QES $|\varphi_\epsilon\rangle$ and the quantum states $|\psi(t_n)\rangle$ of a subsystem with $\lambda = 2$. Here, the time-evolved state is chosen from the region of DL, e.g., $t_n = 100$. Figure 6(b) shows that for $\varepsilon = 0$ the value of $\mathcal{F}$ is almost unity if ϵ_i is maximum (e.g., $\epsilon_i = 32.35$), which demonstrates that the time-evolved state $|\psi(t_n)\rangle$ almost has full overlap with the QES $|\varphi(\epsilon_i = 32.35)\rangle$, which is similar to that of interacting system with $\varepsilon = 5$ in Fig. 6(a). The reason has been revealed in Sec. III. As a further step, we compare the probability density distribution for the four states with maximum $\mathcal{F}$: two QESs $|\varphi_\epsilon\rangle$ with ($\varepsilon = 5$, $\epsilon_i = 64.62$) and ($\varepsilon = 0$, $\epsilon_i = 32.35$); two quantum states $|\psi(t_n = 100)\rangle$ with $\varepsilon = 5$ and $\varepsilon = 0$ in Fig. 6(c). Interestingly, one can see that the profiles of the four states have slight differences, which demonstrates that the quantum state of $\varepsilon = 5$ has a very small difference from that of $\varepsilon = 0$. Such a small difference is also represented by the time evolution of $\langle p^2 \rangle$. The inset of Fig. 6(d) shows the time dependence of $\langle p^2 \rangle$ for $\varepsilon = 0$ and 5, respectively. One can find that for a specific λ value (e.g., $\lambda = 1.5$), $\langle p^2 \rangle$ increases for a very short interval and then saturates, which demonstrates the appearance of DL. Interestingly, the difference of the saturation of $\langle p^2 \rangle$ between $\varepsilon = 0$ and 5 decreases with the increase of λ. To confirm this point, we define the difference of $\langle p^2 \rangle$ as $\Delta_E = \langle p_1^2 \rangle_t - \langle p^2 \rangle_t$, where $\langle p_1^2 \rangle_t$ ($\langle p^2 \rangle_t$) is the time-averaged value of the mean energy, i.e., $\langle p^2 \rangle_t = \int_0^{t_f} \langle p^2 \rangle dt / t_f$ with $\varepsilon = 5$ ($\varepsilon = 0$). We note that in our numerical experiments t_f is on the scale of hundreds of kicking periods due to the very fast saturation of $\langle p^2 \rangle$. Figure 6(d) shows that the difference of Δ_E decreases in power law with λ, i.e., $\Delta_E \approx \lambda^{-\beta}$ with $\beta \approx 0.89$. Therefore, our results present clear evidence that the non-Hermitian kicking potential can effectively lead to the decoupling of the two subsystems.

[1] P. W. Anderson, Phys. Rev. **109**, 1492 (1958).

[2] C. A. Condat and T. R. Kirkpatrick, Phys. Rev. Lett. **58**, 226 (1987).

[3] C. A. Condat and T. R. Kirkpatrick, Phys. Rev. B **36**, 6782 (1987).

[4] A. A. Chabanov, M. Stoytchev, and A. Z. Genack, Nature (London) **404**, 850 (2000).

[5] M. Segev, Y. Silberberg, and D. N. Christodoulides, Nat. Photonics **7**, 197 (2013).

[6] J. Billy, V. Josse, Z. Zuo, A. Bernard, B. Hambrecht, P. Lugan, D. Clément, L. Sanchez-Palencia, P. Bouyer, and A. Aspect, Nature (London) **453**, 891 (2008).

[7] G. Roati, C. D'Errico, L. Fallani, M. Fattori, C. Fort, M. Zaccanti, G. Modugno, M. Modugno,

and M. Inguscio, Nature (London) **453**, 895 (2008).

[8] G. Casati, B. V. Chirikov, F. M. Izrailev, and J. Ford, in *Stochastic Behavior in Classical and Quantum Hamiltonian Systems*, edited by G. Casati and J. Ford, Lecture Notes in Physics, Vol. 93 (Springer, Berlin, 1979).

[9] F. M. Izrailev, Phys. Rep. **196**, 299 (1990).

[10] S. Fishman, D. R. Grempel, and R. E. Prange, Phys. Rev. Lett. **49**, 509 (1982).

[11] F. L. Moore, J. C. Robinson, C. F. Bharucha, B. Sundaram, and M. G. Raizen, Phys. Rev. Lett. **75**, 4598 (1995).

[12] H. Ammann, R. Gray, I. Shvarchuck, and N. Christensen, Phys. Rev. Lett. **80**, 4111 (1998).

[13] M. B. dÁrcy, R. M. Godun, M. K. Oberthaler, D. Cassettari, and G. S. Summy, Phys. Rev. Lett. **87**, 074102 (2001).

[14] C. Ryu, M. F. Andersen, A. Vaziri, M. B. d'Arcy, J. M. Grossman, K. Helmerson, and W. D. Phillips, Phys. Rev. Lett. **96**, 160403 (2006).

[15] I. Talukdar, R. Shrestha, and G. S. Summy, Phys. Rev. Lett. **105**, 054103 (2010).

[16] M. Lopez, J. F. Clement, P. Szriftgiser, J. C. Garreau, and D. Delande, Phys. Rev. Lett. **108**, 095701 (2012).

[17] B. Gadway, J. Reeves, L. Krinner, and D. Schneble, Phys. Rev. Lett. **110**, 190401 (2013).

[18] Z. Wang, W. Fu, Y. Zhang, and H. Zhao, Phys. Rev. Lett. **124**, 186401 (2020).

[19] S. Fishman, Y. Krivolapov, and A. Soffer, Nonlinearity **25**, R53 (2012).

[20] Ch. Skokos, I. Gkolias, and S. Flach, Phys. Rev. Lett. **111**, 064101 (2013).

[21] H. Veksler, Y. Krivolapov, and S. Fishman, Phys. Rev. E **80**, 037201 (2009).

[22] A. Pikovsky and S. Fishman, Phys. Rev. E **83**, 025201(R) (2011).

[23] E. Michaely and S. Fishman, Phys. Rev. E **85**, 046218 (2012).

[24] I. Vakulchyk, M. V. Fistul, and S. Flach, Phys. Rev. Lett. **122**, 040501 (2019).

[25] N. Cherroret, B. Vermersch, J. C. Garreau, and D. Delande, Phys. Rev. Lett. **112**, 170603 (2014).

[26] G. Gligorić, K. Rayanov, and S. Flach, Europhys. Lett. **101**, 10011 (2013).

[27] B. Mieck and R. Graham, J. Phys. A **38**, L139 (2005).

[28] I. Guarneri, Phys. Rev. E **95**, 032206 (2017).

[29] W. L. Zhao, J. Gong, W. G. Wang, G. Casati, J. Liu, and L. B. Fu, Phys. Rev. A **94**, 053631 (2016).

[30] W. Zhao, J. Z. Wang, and W. Wang, J. Phys. A: Math. Theor. **52**, 305101 (2019).

[31] C. Rylands, E. B. Rozenbaum, V. Galitski, and R. Konik, Phys. Rev. Lett. **124**, 155302 (2020).

[32] D. Rossini, G. Benenti, and G. Casati, Phys. Rev. E **74**, 036209 (2006).

[33] J. N. Bandyopadhyay, Europhys. Lett. **85**, 50006 (2009).

[34] S. Adachi, M. Toda, and K. Ikeda, Phys. Rev. Lett. **61**, 659 (1988).

[35] R. Graham and A. R. Kolovsky, Phys. Lett. A. **222**, 47 (1996).

[36] H. K. Park and S. W. Kim, Phys. Rev. A **67**, 060102(R) (2003).

[37] W. L. Zhao and Q. L. Jie, Commun. Theor. Phys. **51**, 465 (2009).

[38] W. L. Zhao, Q. L. Jie, and B. Zhou, Commun. Theor. Phys. **54**, 247 (2010).

[39] W. L. Zhao and Q. L. Jie, Chin. Phys. B **29**, 080302 (2020).

[40] E. B. Rozenbaum and V. Galitski, Phys. Rev. B **95**, 064303 (2017).

[41] J. Wang, G. Benenti, G. Casati, and W. G. Wang, Phys. Rev. E **103**, L030201 (2021).

[42] W. L. Zhao, L. W. Zhou, J. Liu, P. Q. Tong, and K. Q. Huang, Phys. Rev. A **102**, 062213 (2020).

[43] W. L. Zhao, P. K. Gong, J. Z. Wang, and Q. Wang, Chin. Phys. B. **29**, 120302 (2020).

[44] R. El-Ganainy, K. G. Makris, M. Khajavikhan, Z. H. Musslimani, S. Rotter, and D. N. Christodoulides, Nat. Phys. **14**, 11 (2018).

[45] J. Li, A. K. Harter, J. Liu, L. d. Melo, Y. N. Joglekar, and L. Luo, Nat. Commun. **10**, 855 (2019).

[46] Z. Zhang, Y. Zhang, J. Sheng, L. Yang, M.-A. Miri, D. N. Christodoulides, B. He, Y. Zhang, and M. Xiao, Phys. Rev. Lett. **117**, 123601 (2016).

[47] S. Q. Xia, D. Kaltsas, D. H. Song, I. Komis, J. J. Xu, A. Szameit, H. Buljan, K. G. Makris, and Z. G. Chen, Science **372**, 72 (2021).

[48] S. Mukherjee and M. C. Rechtsman, Science **368**, 856 (2020).

[49] S. V. Suchkov, A. A. Sukhorukov, J. H. Huang, S. V. Dmitriev, C. H. Lee, and Y. S. Kivshar, Laser Photonics Rev. **10**, 177 (2016).

[50] Y. Li *et al.*, Science **364**, 170 (2019).

[51] Y. Ashida, Z. Gong, and M. Ueda, Adv. Phys. **69**, 249 (2020).

[52] N. Moiseyev, *Non-Hermitian Quantum Mechanics* (Cambridge University, Cambridge, England, 2011).

[53] K. Q. Huang, J. Z. Wang, W. L. Zhao, and Jie Liu, J. Phys.: Condens. Matter **33**, 055402 (2021).

[54] D. Cohen, Phys. Rev. A **44**, 2292 (1991).

[55] A. Pizzamiglio, S. Y. Chang, M. Bondani, S. Montangero, D. Gerace, and G. Benenti, Entropy **23**, 654 (2021).

[56] C. H. Bennett, G. Brassard, S. Popescu, and B. Schumacher, J. A. Smolin, and W. K. Wootters, Phys. Rev. Lett. **76**, 722 (1996).

[57] G. Saxena, E. Chitambar, and G. Gour, Phys. Rev. Research **2**, 023298 (2020).

[58] E. Chitambar and G. Gour, Rev. Mod. Phys. **91**, 025001 (2019).

[59] N. Anand, G. Styliaris, M. Kumari, and P. Zanardi, Phys. Rev. Research **3**, 023214 (2021).

[60] S. Longhi, Phys. Rev. A **95**, 012125 (2017).

[61] L. W. Zhou and J. X. Pan, Phys. Rev. A **100**, 053608 (2019).

[62] R. Grimaudo, A. Messina, A. Sergi, N. V. Vitanov, and S. N. Filippov, Entropy **22**, 1184 (2020).

[63] N. Okuma and M. Sato, Phys. Rev. B **103**, 085428 (2021).

[64] M. Kreibich, J. Main, H. Cartarius, and G. Wunner, Phys. Rev. A **93**, 023624 (2016).

[65] M. Kreibich, J. Main, H. Cartarius, and G. Wunner, Phys. Rev. A **87**, 051601(R) (2013).

[66] M. Kreibich, J. Main, H. Cartarius, and G. Wunner, Phys. Rev. A **90**, 033630 (2014).

[67] Details of the classical diffusion are shown in Appendix A and a detailed description of the decoupling effects by the non-Hermitian kicking potential is shown in Appendix B.

[68] W. G. Wang, L. He, and J. Gong, Phys. Rev. Lett. **108**, 070403 (2012).

[69] W. G. Wang, Phys. Rev. E **102**, 012127 (2020).

[70] G. M. Bosyk, S. Zozor, F. Holik, M. Portesi, and P. W. Lamberti, Quantum Inf. Process. **15**, 3393 (2016).

[71] H. Zhu, Z. Ma, Z. Cao, S.-M. Fei, and V. Vedral, Phys. Rev. A **96**, 032316 (2017).

[72] C. M. Bender and D. C. Brody, *Optimal Time Evolution for Hermitian and Non-Hermitian Hamiltonians*, edited by J. G. Muga, A. Ruschhaupt, and A. del Campo, Lecture Notes in Physics, Vol. 2 (Springer, Berlin, 2009).

[73] E. M. Graefe, H. J. Korsch, A. Rush, and R. Schubert, J. Phys. A **48**, 055301 (2015).

[74] C. M. Bender, Rep. Prog. Phys. **70**, 947 (2007).

[75] C. M. Bender, J. Feinberg, D. W. Hook, and D. J. Weir, Pramana **73**, 453 (2009).

[76] C. M. Bender, S. Boettcher, and P. N. Meisinger, J. Math. Phys. **40**, 2201 (1999).

[77] C. M. Bender and D. W. Hook, J. Phys. A **44**, 372001 (2011).